Materials Science Applications of X-Ray Diffraction

Åke Kvick, European Synchrotron Radiation Facility, Grenoble, France

© 1999 Elsevier Ltd. All rights reserved.

This article is reproduced from the previous edition, volume 2, pp 1248–1257, © 1999, Elsevier Ltd.

Symbols

A	atomic weight
B_i	background in point i
C_d	concentration of dopant
C, D, σ_{N-K}, N	constants
C_{ijkl}	elastic stiffness constants
d	atomic spacing
D	particle size
E	Young's modulus
E_k	kth component of electric field
f_j	atomic scattering factors
F_{hkl}	amplitude structure factors
g	powder peak shape function
I	intensity of beam
I_0	incident intensity of beam
j,k	satellite order number
K	constant
N	normalization factor
N	number of atoms
R	tetrahedral radius
s_{ijkl}	elastic compliances
t	thickness of sample
u_j, v_j, w_j	fractional coordinates for atom j
ν	Poisson's ratio
V_c	volume of unit cell
W	weight factor
Y_i	deconvolution function
Z	atomic number
δ_{ij}	Kronecker delta
$\Delta\theta$	change of angle of scattering
ε	elastic strain coefficient
θ	angle of scattering
λ	wavelength
Λ	periodicity of superlattices
μ	absorption coefficient
ρ	density
$\rho(xyz)$	electron density distribution
σ_n	absorption cross-section for component n
σ	stress
τ	penetration distance
φ	angle
ϕ	phase

The X-ray diffraction technique is widely used in structural characterization of materials and serves as an important complement to electron microscopy, neutron diffraction, optical methods and Rutherford backscattering.

The early uses were mainly in establishing the crystal structures and the phase composition of materials but it has in recent years more and more been used to study stress and strain relationships, to characterize semiconductors, to study interfaces and multilayer devices, to mention a few major application areas.

One of the important advantages of X-ray diffraction is that it is a nondestructive method with penetration from the surfaces into the bulk of the materials. This article will outline some of the most important areas including some rapidly developing fields such as time-dependent phenomena and perturbation studies.

X-ray Sources

X-rays are electromagnetic in nature and atoms have moderate absorption cross-sections for X-ray radiation resulting in moderate energy exchange with the materials studied, making diffraction a nondestructive method, in most cases.

Traditionally X-rays are produced by bombarding anode materials with electrons accelerated by a >30 kV potential. The collision of the accelerated electrons produces a line spectrum superimposed on a continuous spectrum called *bremsstrahlung*.

The line spectrum is characteristic of the bombarded anode material and has photon intensities much higher than the continuous spectrum. The characteristic lines are generated by the relaxation of excited electrons from the electron shells and are labelled K, L, M, etc. and signify the relaxation L to K, M to K, etc.

A table of available laboratory wavelengths is given in Table 1.

The increased importance of X-ray diffraction in materials science is coupled to the emergence of a new source of X-rays based on *synchrotron radiation* storage rings. The synchrotron radiation is produced by the bending of the path of relativistic charged particles, electrons or positrons, by magnets causing an emission of intense electromagnetic radiation in the forward direction of the particles. The photons are generated over a

Table 1 Radiation from common anode materials

Radiation	*Wavelength (Å)*	*Energy (keV)*
Ag K_α	0.5608	22.103
Pd K_α	0.5869	21.125
Rh K_α	0.6147	20.169
Mo K_α	0.7107	17.444
Zn K_α	1.4364	8.631
Cu K_α	1.5418	8.041
Ni K_α	1.6591	7.742
Co K_α	1.7905	6.925
Fe K_α	1.9373	6.400
Mn K_α	2.1031	5.895
Cr K_α	2.2909	5.412
Ti K_α	2.7496	4.509
Synchrotron	~0.05–3	4.300

The value α is a mean of the $K_{\alpha 1}$ and $K_{\alpha 2}$ emissions. The synchrotron radiation is continuous and the range is the most commonly used. The range may be extended on both sides.

Figure 1 Beam lines at the European Synchrotron Radiation Facility in Grenoble, France.

wide energy range from very long wavelengths in the visible to hard X-rays up to several hundred keV.

The radiation is very intense and exceeds the available normal laboratory sources by up to 6 or 7 orders of magnitude. The synchrotron storage rings used for the radiation production, however, are large and expensive, with facilities characterized by storage rings with a circumference up to more than one thousand metres.

The main advantages of synchrotron radiation are:

1. continuous radiation up to very high energies (>100 keV);
2. high intensity and brightness;
3. pulsed time structure down to picoseconds;
4. high degree of polarization.

Figure 1 illustrates a modern synchrotron facility with many experimental facilities in a variety of scientific areas from atomic physics to medicine.

Figure 2 compares the brightness of the available X-ray sources.

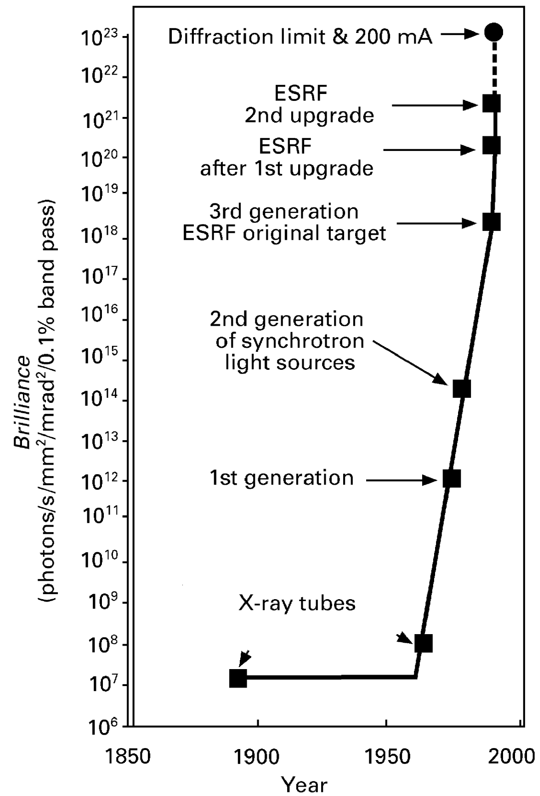

Figure 2 The brightness defined as photons/s/mm^2/mrad^2/0.1% energy band pass for conventional and synchrotron X-ray sources. ESRF denotes the European Synchrotron Radiation source in Grenoble, France.

X-ray Diffraction

The diffraction method utilizes the interference of the radiation scattered by atoms in an ordered structure and is therefore limited to studies of materials with long-range order.

The incoming X-ray beam can be characterized as a plane wave of radiation interacting with the electrons of the material under study. The interaction is in the form of both absorption and scattering. The scattering can be thought of as spheres of radiation emerging from the scattering atoms. If the atoms have long-range order, the separate 'spheres' interfere constructively and destructively producing distinct spots, *Bragg reflections*, in certain directions.

The specific scattering angles, θ_{hkl}, carry information on the long-range ordering dimensions and the intensity gives information on the location of the electrons within that order.

The basis for all material science studies using X-ray diffraction is Bragg's law:

$$\lambda = 2d_{hkl}\sin(\theta_{hkl}) \qquad [1]$$

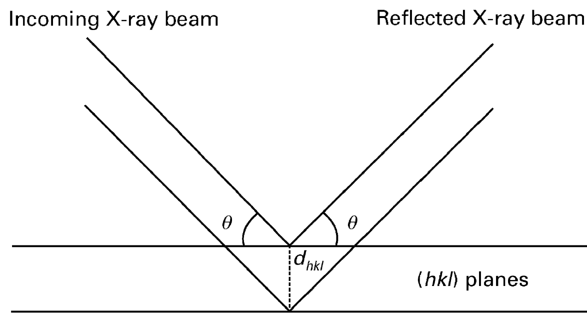

Figure 3 Reflection from the planes (*hkl*) with interplanar spacing d_{hkl}.

where λ is the wavelength of the incoming radiation, d_{hkl} is the spacing of the (hkl) atomic plane and θ is the angle of the diffracting plane where constructive interference occurs (see Figure 3).

Differentiation of Bragg's law gives the expression:

$$\Delta(\theta) = -\Delta(d)/d\tan(\theta) \qquad [2]$$

which is an important formula relating the observed changes in scattering angles to structural changes in the material.

The penetration depth of the probing radiation is an important parameter in designing a diffraction experiment. The penetration depth is associated with the absorption of the radiation, which is a function of the absorption cross-section of the material under study. The absorption can be calculated by the formula:

$$I/I_0 = \exp(-\mu t) \qquad [3]$$

where I_0 is the intensity of the incident beam and I is the intensity of a beam having passed through t (cm) of material with an absorption coefficient of μ (cm^{-1}).

The absorption coefficient μ can be calculated as an additive sum over the different atomic species in the unit cell:

$$\mu = 1/V_c \sum(\sigma_n) \qquad [4]$$

where V_c is the volume of the unit cell and σ_n is the absorption cross-section for component n. The absorption cross-sections vary as a function of the wavelength and can be calculated using the Victoreen expression:

$$\mu/\rho = C\lambda^3 - D\lambda^4 + \sigma_{K-N}NZ/A \qquad [5]$$

where ρ is the density of the material with atomic number Z and the atomic weight A. The constants C, D and $\sigma_{K-N}N$ vary with the wavelength. Tabulations for various materials can be found in International Tables for Crystallography, Vol III, pp 161 ff.

Table 2 Penetration depth τ (1/e) in Al, Fe and Cu for various techniques in millimetres

	Al	*Fe*	*Cu*
Scanning electron microscope	<0.001	<0.001	<0.001
X-ray diffraction (Cu K_α)	0.14	0.007	0.005
Synchrotron X-rays (80 keV)	18	2.1	1.4
Synchrotron X-rays (300 keV)	36	11.5	10
Neutrons (cold)	97	8.3	10

It can be noted that the absorption drops off with decreasing wavelength and the penetration depth can thus be changed with a change in wavelength. A quantity called *penetration distance*, τ, is usually quoted for penetration depths and is defined as the distance where I/I_0 is reduced to 1/e. Penetration distances for a few elements are listed in Table 2, together with a comparison with other methods.

Structure Determinations

Historically, and even today, the structure determination of crystalline materials is the most important application of X-ray diffraction in materials science. The relative intensities of Bragg reflections carry information on the location of the electrons in the solids and thus give precise information on the relative positions and thermal motion of the atoms. Even information on the bonding electrons may be obtained.

The scattered intensities from different planes (*hkl*) in a crystal are measured using precise diffractometers that orient the sample with respect to the incident X-ray beam for all the possible diffraction planes in the crystal. Intensities are measured using scintillation, semiconductor CCD or imaging plate detectors. The measured intensities are converted, after various geometric corrections, to the amplitude structure factors $|F_{hkl}|$ which are proportional to the scattered intensities.

The factors can be expressed as:

$$F_{hkl} = \sum^{j} f_j \exp\{-2\pi i(hu_j + kv_j + lw_j)\} \qquad [6]$$

where the f_j are the atomic scattering factors for atoms j and u_j, v_j and w_j are the fractional coordinates for atom j.

The electron density in the crystal unit cell can be determined from the structure factors $F_{hkl} = |F_{hkl}| \times e^{i\varphi hkl}$. The structure amplitudes ($|F_{hkl}|$) are obtained from the experiments and the phases φ can be obtained from a number of phasing procedures. The structure factors can then be converted to a mapping of the electron density distribution $\rho(xyz)$, which

completely determines the crystal structure.

$$\rho(xyz) = 1/V_c \sum^{hkl} |F_{hkl}| e^{i\varphi hkl} \exp(-2\pi(hx + ky + lz)) \quad [7]$$

V_c is the volume of the unit cell and x,y,z are the positional coordinates in the unit cell.

The most precise structure determinations are performed using a single crystal sample where hundred to thousands of separate Bragg spots can be used to determine atomic positions to a precision of better than 0.001 Å. In materials science, however, quite frequently the material is in a polycrystalline form and powder diffraction methods have to be employed.

In the powder diffraction method the Bragg reflections from many thousands of microcrystals with different orientation overlap giving rise to 'powder' diffraction rings rather than distinct Bragg spots. Since the powder patterns are in the form of rings rather than distinct spots (see **Figure 4**) the observed intensities from planes with identical or closely similar scattering angles are analysed in terms of a deconvolution function:

$$Y_i = B_i + \sum^{hkl} I(hkl)Ng \quad [8]$$

where B_i is the background in point i, g is the powder peak shape function and N is a normalization factor. Once a structure model is obtained a refinement procedure proposed by Rietveld can be used to minimize the quantity

$$M = \sum^{i} W(Y_i(\text{obs}) - Y_i(\text{calc}))^2 \quad [9]$$

where W is a weight factor based on counting statistics. Y(calc) may contain positional, thermal parameters, unit cells as well as peak shapes and these parameters are refined during the minimization.

The method is used for structure determinations and is well suited to handling multiphase systems. At present the method gives bond distances to within ≥ 0.005 Å precision, and *ab initio* structure determinations may handle systems with up to 200 parameters. **Figure 5** gives an example of a powder pattern collected at the European Synchrotron Radiation Facility of a two-phase powder sample.

The broadening of a diffraction line may give important information on changes occurring during the processing of the material. The line width is affected

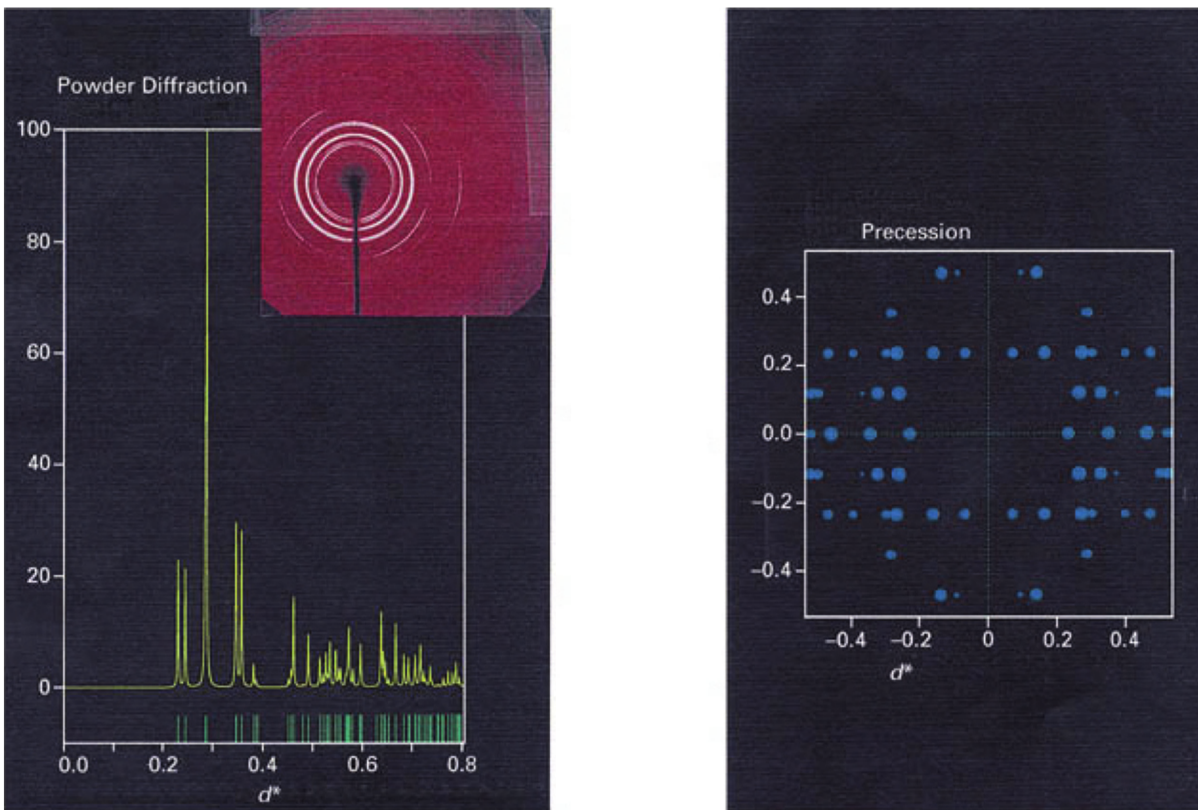

Figure 4 The left-hand picture illustrates a powder diffraction pattern of S_2N_2 at a wavelength of 0.325 Å. The inset is the actual pattern which can be integrated and displayed as a function of d^* [$d^* = (2\sin\theta)/\lambda$]. The right-hand picture shows the result if one single S_2N_2 crystal is rotated in the X-ray beam. The size of the spots illustrates the difference in diffracted intensities from the separated Bragg reflections. Courtesy of Svensson and Kvick, 1998.

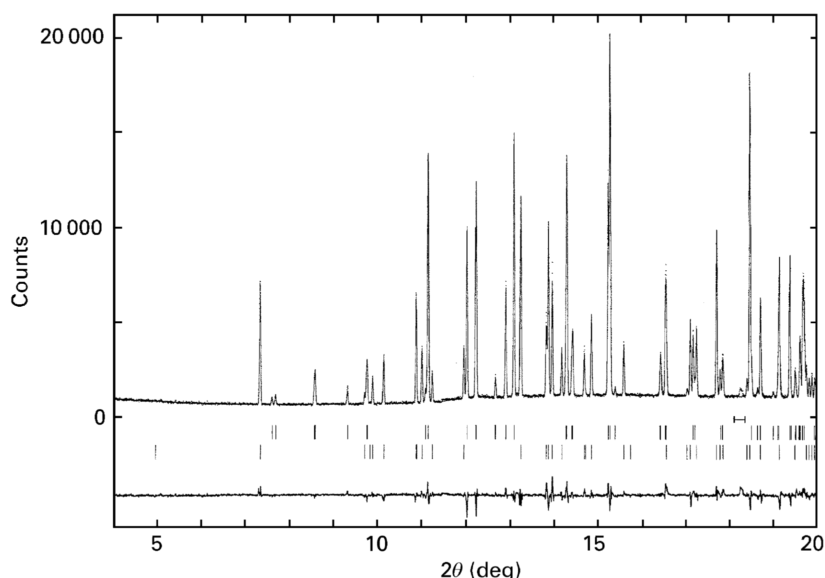

Figure 5 The powder pattern from a two-phase mixture of orthorhombic $(CH_3)_2SBr_{2.5}$ and monoclinic $(CH_3)_2SBr_4$ recorded at a wavelength of 0.94 718 Å at the BM16 beamline at the ESRF. The two lines of vertical bars show the location of diffraction lines for the two different phases. The bottom pattern shows the difference between the observed and refined intensities from the Rietveld refinement. Courtesy of Vaughan, Mora, Fitch, Gates and Muir, 1998.

by instrumental resolution, source size, divergence of the radiation, particle size, microstrain components and stacking faults. After appropriate correction qualitative information on the micrograin size can be obtained by using the Scherrer formula. The grain size affects the line broadening as a function of wavelength and scattering angle as:

$$\Delta 2\theta = \lambda/(D\cos\theta) \qquad [10]$$

where D is the particle size.

In order to separate particle broadening from strain effects two or more reflections may be used. The strain varies as function of tanθ and the different effects in line broadening may thus be separated by determining the broadening from different (hkl) diffraction lines.

Anomalous Scattering

The absorption and scattering can change considerably around the absorption edges for the atoms. The absorption edge region is the atom specific energy region where the inner electrons are sufficiently excited by the X-rays to leave the atom or to be excited to an upper electronic shell. In this region the atomic scattering factor f_j is modified and is no longer a real property but has, in addition to an extra real term f'_j, an imaginary term f''_j.

The term in eqn [6] changes to:

$$f_j = f_j^0 + f'_j + \mathrm{i}f''_j \qquad [11]$$

These changes can be used to alter the absorption and consequently the penetration depth by changing the wavelength around the absorption edges. The changes may be considerable and can amount to the equivalence of tens of electrons.

In addition to changes in absorption there are fundamental differences in the scattering which may be used in materials science. Examples include the determination of absolute optical configuration in polar compounds.

Normally, the Friedel pairs of structure factors, i.e. $F(hkl) = F(-h\text{–}k\text{–}l)$, are identical. However, around the absorption edges this law breaks down since the imaginary term adds differently in the phase relation and the correct optical isomer can be determined.

The alternation of the scattering for a specific atom may also be used to resolve the partial contribution of that atom at a specific site by multiple wavelength differences studies.

The scattering contrast between almost isoelectronic elements such as Fe and Co may be enhanced sufficiently to allow precise determinations. Small chemical shifts in the energy of the edges depending on the valence state of the atom may also be used to differentiate between the valence states of the atoms in a compound.

The effect is particularly useful for structure determinations of macromolecules where multiple anomalous diffraction (MAD) experiments are combined to yield the phase factors necessary to obtain the electron density mapping.

The use of anomalous diffraction has gained in importance as synchrotron radiation sources have

become available. The synchrotron sources provide easily tuneable radiation covering most of the atomic absorption edges.

Magnetic Scattering

The minute scattering component coming from the magnetic moments of atoms has been exploited more recently. The scattering from the magnetic moments are smaller than the scattering from the electrons by orders of magnitude. However, successful studies of magnetic structures and even magnetic atomic overlayers are now possible by using the high brightness synchrotron sources.

The synchrotron radiation also makes it possible to tune the wavelength to the absorption edges of the magnetic atoms where the magnetic scattering is strongly enhanced. For a more detailed account of anomalous diffraction and magnetism the reader is referred to the book edited by Materlik and co-workers (1994).

Stress and Strain Relationships

Elastic X-ray stress analysis is based on recordings of the interplanar distances d_{hkl}. When stress is applied to a crystal the distances change from d_0 to $d_0 + \Delta d$ and the scattering in Bragg's law (eqn [1]) will change accordingly. Using eqn [2] one obtains the relationship:

$$\Delta\theta = (\theta - \theta_0) = -\Delta d/d_0 \tan(\theta_0) = -\tan(\theta_0)\varepsilon \qquad [12]$$

where θ_0 is the scattering angle from a strain-free state, and ε is the elastic strain coefficient. θ is obtained from the diffraction experiment.

In strain analysis the formalism given by Noyen and Cohen (1976) can be used where the strain in the direction of a scattering plane (hkl) is measured as:

$$\varepsilon'(33)_{\phi\varphi} = (d_{\phi\varphi} - d_0)/d_0 \qquad [13]$$

The plane spacing d_0 is measured from a strain-free sample.

To obtain the strain in the sample system S one transforms the values from the laboratory coordinate system L.

The orthogonal coordinate systems S_1,S_2,S_3 and L_1,L_2,L_3 are defined as follows. S_3 is perpendicular to the sample surface and S_2 and S_3 are parallel to the sample surface. L_3 is the normal to the scattering plane hkl and makes the angle φ with S_3. The ϕ angle is the angle between the projection of L_3 onto the sample surface and vector S_1. The measured quantity $\varepsilon_{\phi\varphi}$ can then be converted to the sample coordinate system by the transformation:

$$\begin{aligned}\varepsilon'(33)_{\phi\varphi} = {} & \varepsilon_{11}\cos^2\phi\sin^2\varphi + \varepsilon_{12}\sin2\phi\sin^2\varphi \\ & + \varepsilon_{22}\sin^2\phi\sin^2\varphi\varepsilon_{33}\cos^2\varphi + \varepsilon_{13}\cos\phi\sin^2\varphi \\ & + \varepsilon_{23}\sin\phi\sin^2\varphi \end{aligned} \qquad [14]$$

This important equation is linear in ε_{11}, ε_{12}, ε_{22}, ε_{33}, ε_{13}, ε_{23} and these coefficients can thus be determined from six measurements at different angular values. When this is known the stress can be determined.

The stress (σ) and strains (ε) in the sample coordinate system are determined using Hooke's law:

$$\begin{aligned}\sigma_{ij} &= c_{ijkl}\,\varepsilon_{kl} \\ \varepsilon_{ij} &= s_{ijkl}\,\sigma_{kl}\end{aligned} \qquad [15]$$

where the c_{ijkl} are the elastic stiffness constants and s_{ijkl} are the elastic compliances.

In the elastic case the observations may be expressed in terms of Young's modulus E and Poisson's ratio ν:

$$(d_{\phi\varphi} - d_0)/d_0 = (1 + v/E)\sigma_{ij} - (\delta_{ij}v/E)\sigma_{kk} \qquad [16]$$

where δ_{ij} is the Kronecker delta.

This formalism is the basis for the commonly used $\sin^2\varphi$ method, which is usually limited to the surface region of the sample.

The availability of more elaborate diffractometers and the highly penetrating synchrotron radiation also gives possibilities of deeper penetration into the sample by rotation of the sample around the scattering vector direction, L_3, and by wavelength tuning or change in the scattering angle. Transmission studies permit the study of stresses in specific 'gauge' volumes in the bulk.

Externally Perturbed Systems

Deformations due to perturbations may also be followed by X-ray diffraction.

These perturbations may be caused by electric field or changes in temperature and thus piezoelectric effects and thermal expansion coefficients may readily be determined by using eqn [2].

In the case of changes occurring from the application of an external electric field, the converse piezoelectric effect, the induced strain coefficient ε_{ij} is related to the field by equation:

$$\varepsilon_{ij} = \sum_{k=1}^{3} d_{kij}E_k \qquad [17]$$

where E_k is the kth component of the electric field and d_{kij} is the kijth element of the third rank piezoelectric tensor.

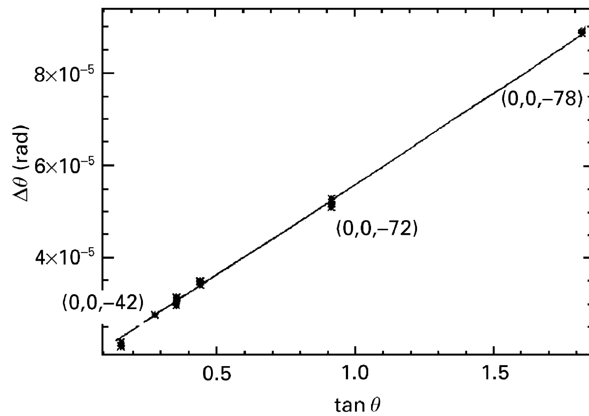

Figure 6 The shifts in $\Delta\theta$ for (00*l*) reflections from a $LiNbO_3$ single crystal of 0.2 mm thickness subjected to an electric field of 50 kV cm^{-1} along the crystallographic *c* direction as measured using synchrotron radiation of a wavelength of 0.307 Å at the beamline 1D11 at the ESRF. The d_{33} element of the piezoelectric tensor can be evaluated to be $7.5(2)\times10^{-12}$ CN^{-1}. Courtesy of Heunen, Graafsma, Kvick, 1997.

Using eqn [2] Barsch has shown that the diffraction observable $\Delta\theta_r$ may be used to determine the piezoelectric tensor according to the formula (Coppens, 1992):

$$\Delta\theta_r = -E\tan\theta_r \sum_{k=1}^{3}\sum_{i=1}^{3}\sum_{j=1}^{3} e_k\, h_{r,i}\, h_{r,j}\, d_{kij} \qquad [18]$$

where r refers to certain reflections (*hkl*) and e_k, $h_{r,i}$ and $h_{r,j}$ are, respectively, the components of unit vectors parallel to the electric field and the scattering vector for (*hkl*).

Figure 6 gives an illustration where the piezoelectric tensor element d_{33} has been determined from measurements of a series of 00*l* reflections with the electric field aligned along the (00*l*) direction.

Ion-Implantation Effects

Ion implantation in layers of semiconductor material is an important process where eqn [2] may be very useful for assessing the effect on the implantation.

If dopants are introduced by ion implantation, for instance in silicon, the tetrahedral radius of the dopant (r_d) differs from that of the substrate and changes in the θ angle will be observed.

For cubic silicon material the corresponding change in the unit cell dimension can give information on the doping level according to Vegard's law:

$$\Delta a/a = (1 - r_d/r_s)KC_d N^{-1} \qquad [19]$$

where r_d and r_s are the tetrahedral radii of the dopant and substrate respectively, C_d is the concentration of dopant and N is the number of substrate of atoms per unit volume.

The factor K takes account of the fact that only the lattice strain normal to the wafer is nonzero, whereas the in-plane strain is zero. For typical substrates with cubic structure the K values can be evaluated from the elastic stiffness constants.

Superlattice Structures

Physical properties of materials may be changed by creating 'artificial' structural periodicity by depositing alternate thin layers of different materials. Structures of this type are commonly used in optics, electrooptical applications and coatings for corrosion protection or thermal barriers.

The production and performance of these structures can be characterized by X-ray diffraction. The diffraction patterns from the compound structures are characterized by main diffraction peaks interspersed by satellite peaks. The periodicity of superlattices, Λ, is given by the relationship:

$$\Lambda = (j - k)\ \lambda/2(\sin\theta_j - \sin\theta_k) \qquad [20]$$

where j and k represent the satellite order number and θ_j and θ_k are the observed scattering angles at wavelength λ. The periods may vary depending on the production and the variation can be monitored by the various Λ values obtained from different satellite pairs. These period variations may be interpreted as surface roughness.

Topography

Diffraction topography is an imaging technique based on Bragg's law (eqn [1]) and ranges from a rather qualitative inspection method of the scattering power over a crystal to a much more complicated method employing dynamical scattering theory to elucidate microscopic strains in the crystal. Many phenomena of importance to a materials scientist, such as stacking faults, growth bands, strain around grain boundaries, twins, or even dynamical phenomena such as acoustic waves or magnetic domain formation, have been studied by this method.

The studies can be divided into two main areas:

(a) orientation contrast;
(b) extinction contrast.

The former studies (a) map the variation of the scattering power across the X-ray beam and detect misalignment of certain portions of the crystal where the misalignment is larger than the divergence of the monochromatic incident beam. The misalignment can be due to rotations or dilations of the lattice. When

monochromatic radiation is used these effects are seen as distinct bands or patterns of *loss* of scattered radiation.

A richer pattern of intensity variations is seen if continuous wavelength radiation is used. In this case, due to divergence or convergence of the diffracted beams at the boundaries, *losses and gains* in intensity are observed.

The second phenomenon (b) is observed when the scattering power in the crystal is alternated by strain fields around defects without major realignment in the crystal.

The observed contrasts are rather complicated to quantify and an understanding of the effects of the X-ray wavefields is necessary to interpret the observations in detail. For a detailed account of the theory the reader is referred to Tanner (1976).

Topography uses two different methods of observation; reflection topography, which maps the surface region of the samples, and transmission topography, which also samples the bulk of the material. In the latter case the radiation must be chosen so that the absorption is small enough to allow bulk penetration.

Different volumes in the crystal may be sampled if the collimation of the incident and diffracted beams is carried out carefully. This method is called section topography.

Figure 7 gives an example of the information one may obtain from a transmission topograph.

Time-Resolved Studies

Time-resolved X-ray diffraction has been used for a long time to study solid-state reactions. With the emergence of the new radiation sources it is now possible to follow solid-state reactions, phase transitions and physical changes caused by perturbations on much shorter time-scales.

Topography has already proved to be a suitable technique for studying magnetic domain formation or acoustic deformation down to time-scales of milliseconds.

The use of well-collimated and high-intensity synchrotron radiation beams is essential to reach the necessary time intervals without losing the statistical significance in the observed diffracted intensities. The white beam Laue technique has already been proven to facilitate studies down to the picosecond time regime for studies such as recombination of CO in myoglobin after flash photolysis. Nanosecond resolution has been obtained in a study of laser-annealing of defects in a silicon crystal.

The dynamics of reactions are either reversible or irreversible. Sufficient counting statistics can be obtained in the reversible processes through stroboscopic measurement where repeated measurements using short radiation time slices are performed. In the irreversible experiments the processes have to be followed by rapid consecutive exposures.

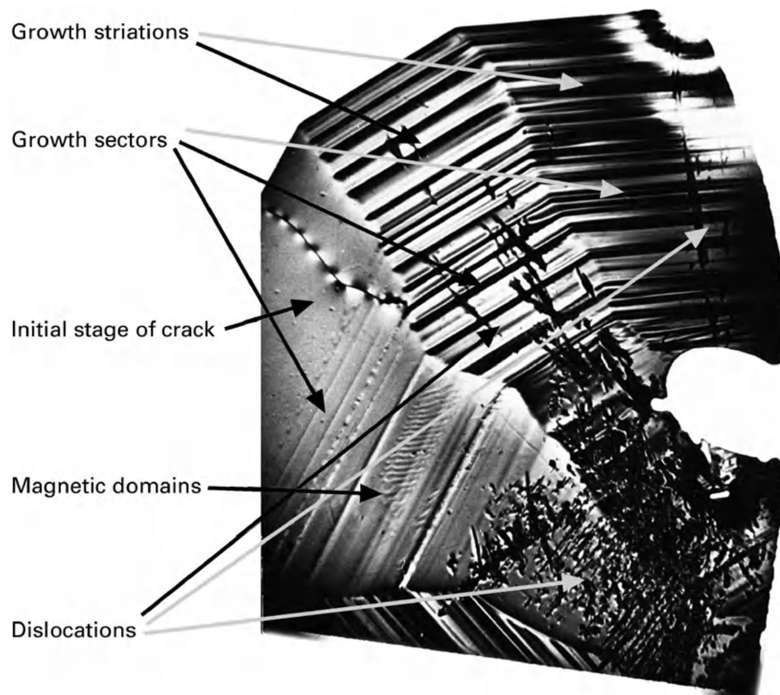

Figure 7 Transmission topograph of a flux grown Ga-YIG ($Y_3Fe_{5-x}Ga_xO_{12}$, $x \approx 1$) crystal plate, Mo $K_{\alpha 1}$-radiation ($\lambda = 0.709$ Å). Courtesy of J Baruchel, 1998.

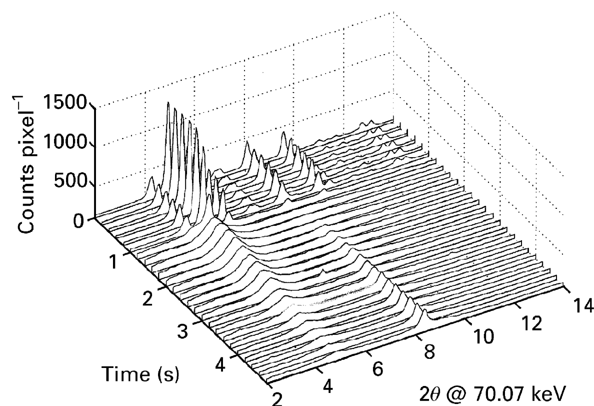

Figure 8 The time-evolution of the powder pattern of an exothermic reaction of a mixture of Al and Ni powders. The powder patterns were recorded at the 1D11 beam line at the ESRF every 250 ms during the self-propagating high-temperature synthesis. The wavelength 0.177 Å was chosen to allow penetration of the sample. It can be noticed that the original peaks from Al and Ni disappear or change during the reaction and the formation of new phases and the nucleation can be followed. Courtesy of Kvick, Vaughan, Turillas, Rodriguez, Garcia, 1998.

In many of the cases the reactions are often destructive to large single crystals and the powder method has to be employed. However, it has been proven that reactions such as polymerization and exothermic solid-state reactions may be followed down to the millisecond time-regime even when the reactions are irreversible.

Figure 8 exemplifies the time-evolution of an exothermic reaction between Al and Ni powders. In this time-resolved powder experiment one can follow the initial melting of Al and the formation of intermetallic phases as well as the crystallization process.

The rapid development of fast read-out CCD cameras in combination with the high brightness synchrotron sources promises to give X-ray diffraction a prominent role in the studies of dynamics of processes relevant to materials scientists.

See also: Fibres and Films Studied Using X-Ray Diffraction, Powder X-Ray Diffraction, Applications, Scattering and Particle Sizing Applications, Scattering Theory.

Further Reading

Authier A, Lagomarsino S, and Tanner B (1996) *X-ray and Neutron Dynamical Diffraction*. New York and London: Plenum Press.

Coppens P (1992) *Synchrotron Radiation Crystallography*. London, San Diego: Academic Press.

International Tables for Crystallography, vol. I–III (1989) Dordrecht, Boston, London: Kluwer Academic Publishers.

International Tables for Crystallography, vol. A–C (1992) Dordrecht, Boston, London: Kluwer Academic Publishers.

Materlik G, Sparks CJ, and Fischer K (1994) Amsterdam, London, New York, Tokyo: North-Holland.

Noyan IC and Cohen JB (1987) *Residual Stress*. New York, Berlin, Heidelberg, London, Paris, Tokyo: Springer-Verlag.

Tanner BK (1976) *X-ray Diffraction Topography*. Oxford: Pergamon Press.